Bull. Mater. Sci., Vol. 29, No. 4, August 2006, pp. 347–355. © Indian Academy of Sciences.

Impedance and a.c. conductivity studies on $Ba(Nd_{0.2}Ti_{0.6}Nb_{0.2})O_3$ ceramic prepared through conventional and microwave sintering route

SYED MAHBOOB, G PRASAD and G S KUMAR*

Department of Physics, Osmania University, Hyderabad 500 007, India

MS received 7 October 2005; revised 9 May 2006

Abstract. Electrical conduction studies on $Ba(Nd_{0.2}Ti_{0.6}Nb_{0.2})O_3$ ceramic samples prepared through conventional and microwave sintering route are presented in this paper. D.C. and a.c. conductivities of these samples as a function of temperature from 300–900 K have been studied. Two types of conduction processes are evident from the frequency dependant conductivity plots, i.e. low-frequency conduction due to short-range hopping and high-frequency conduction due to the localized relaxation (reorientational) hopping mechanism. Grain and grain boundary contributions to the conductivity in these samples are obtained from impedance/admittance measurements via equivalent circuit modelling.

Keywords. Barium titanate; impedance; grain/grain boundary resistance and capacitance; grain/grain boundary relaxation frequency; electrical conductivity; hopping mechanism.

1. Introduction

$BaTiO_3$ is a ferroelectric material with perovskite structure. It finds widespread applications as a capacitor material because of its high permittivities ($\sim 10^3$). There is an enormous literature on the homovalent, heterovalent ions doped in $BaTiO_3$ and sodium bismuth titanate either at A or B-site or at both sites, and solid solution of $BaTiO_3$ with other perovskite materials, which shows relaxor dielectric behaviour and some of these materials show good electrostrictive strains (Park *et al* 1999; Chen *et al* 2000; Yu *et al* 2000; Senda and Mercurio 2001; Suchanicz *et al* 2001; Sheets *et al* 2001; Wang *et al* 2003). Our earlier studies on dielectric behaviour of Nd and Nb doped $BaTiO_3$ at B site showed relaxor behaviour. Substitution of Nd and Nb at B site in $BaTiO_3$ has decreased the transition temperature when compared to the tetragonal–cubic transition temperature of normal $BaTiO_3$ (120°C) (Mahboob *et al* 2005).

A.C. impedance analysis has proved to be a powerful technique to estimate the influence of grain, grain boundary and electrode effects on the charge transport phenomenon in perovskite materials (Sinclair and West 1989a, b; Seok and Kim 1999). These studies also reveal the polarization effects in the material.

Most of the earlier investigations on ferroelectric materials (Buchanan 1988) described the electrical conductivity in terms of electrons (or holes), polarons, oxygen vacancies, impurities and thereby the mechanism of ionic conductivity was established on firm footing. In order to understand the mechanism of charge transport, d.c. and a.c. conductivity studies were carried out over a wide range of temperatures on the present sample.

The aim of the present work is to study the electrical properties of conventional and microwave sintered $Ba(Nd_{0.2}Ti_{0.8}Nb_{0.2})O_3$ sample over a wide range of frequency and temperature (300–900 K) and to investigate the conduction mechanism and also to understand the processing parameters on conduction mechanism.

2. Experimental

$Ba(Nd_{0.2}Ti_{0.6}Nb_{0.2})O_3$ ceramic was prepared by conventional solid state reaction of carbonate ($BaCO_3$, 99·9%, Merck) and oxides (Nd_2O_3, 99·9%, Rare Earths India Ltd., Nb_2O_5, 99+%, Nuclear Fuel Complex, India; and TiO_2, 99·99%, Sigma Aldrich). The required stoichiometric mixtures of the weighed ingredients were intimately mixed and ground in an agate mortar and pestle. The powder was calcined at 1150°C for 2 h. The calcined powder was once again thoroughly mixed and ground for 2 h. Finally cylindrical pellets of 1 mm thickness were prepared by pressing powder to 2–3 tons/cm^2 in a 10 mm diameter stainless steel die using hydraulic press. Prior to pressing, polyvinyl alcohol was added to powder to bind the particles and to reduce the friction between die-wall and sample surface. The pellets were conventionally sintered at 1400°C for 2 h. Microwave sintering was done at 1500°C for 1 h using household microwave oven suitably modified with temperature controller to control the temperature, dimmerstat to regulate the input power etc.

*Author for correspondence (gskumar1948@sify.com)

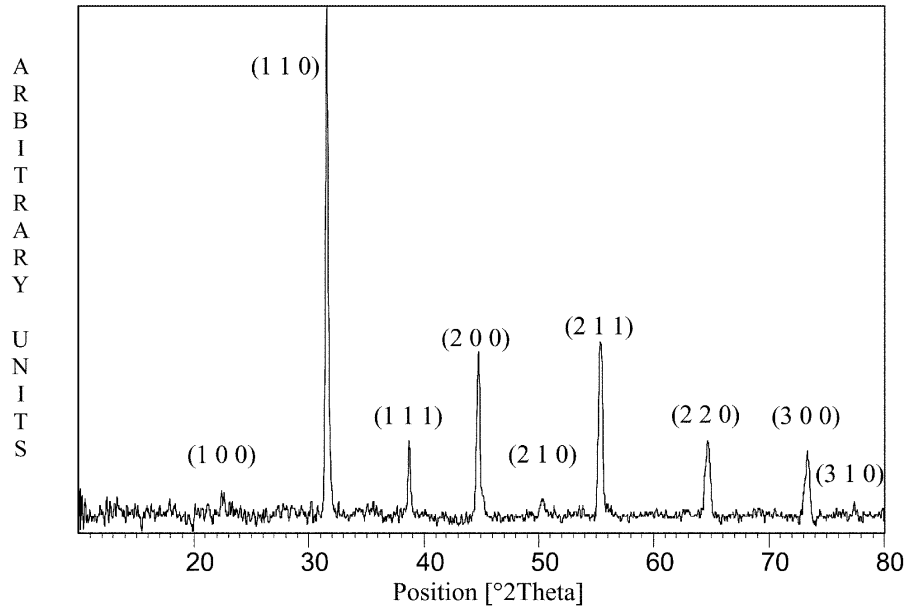

Figure 1. XRD of $Ba(Nd_{0·1}Ti_{0·8}Nb_{0·1})O_3$ sample.

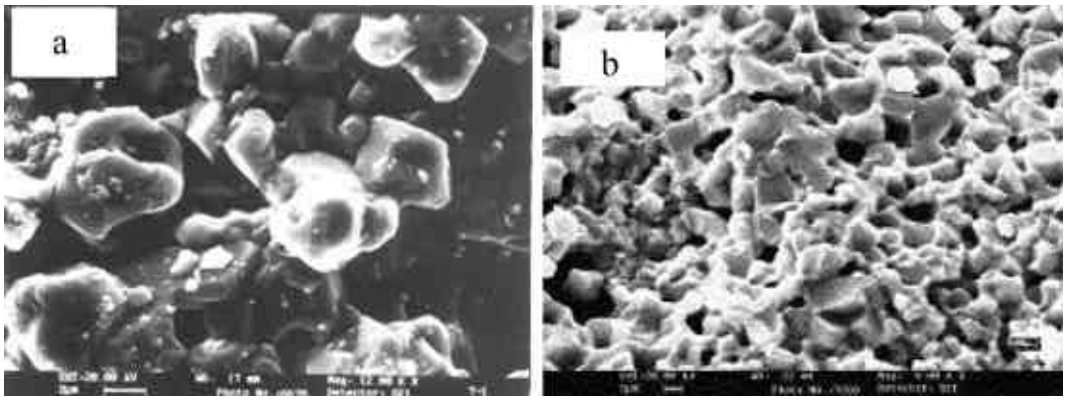

Figure 2. Scanning electron microscopic (SEM) graphs of fractured surfaces of **a**. CS $Ba(Nd_{0·2}Ti_{0·6}Nb_{0·2})O_3$ sample and **b**. MWS $Ba(Nd_{0·2}Ti_{0·6}Nb_{0·2})O_3$ sample.

X-ray powder diffractometer model PW3040/60 X'pert PRO was used to confirm the formation of single-phase. The grain size distribution and morphology were determined by using scanning electron microscope (SEM model LEICA S430).

For impedance and conductivity measurements, both the large surfaces of the samples were electroded with silver paint. Frequency and temperature dependent impedance properties were measured using AUTOLAB (PGSTAT 30) low frequency impedance analyser interfaced to a PC using frequency response analyser software. Temperature dependant d.c. conductivity measurements were done using Keithley 610C electrometer.

3. Results and discussion

Single-phase formation of $Ba(Nd_{0·2}Ti_{0·6}Nb_{0·2})O_3$ ceramics is confirmed through X-ray diffraction (figure 1). The X-ray pattern is indexed based on the cubic structure of $BaTiO_3$ and the lattice parameter is found to be 4·1197 Å. The experimental density of the conventional sintered (CS) sample is 5·794 g/cc and microwave sintered (MWS) sample is 5·554 g/cc, which are 94 and 90% of theoretical X-ray density. SEM graphs of the fractured surface of CS and MWS samples are shown in figures 2a and b, respectively. No secondary phase was observed in the SEM graphs. The average grain size of the CS samples is found to be between 2 and 3 μm and MWS sample to be between 1 and 2 μm.

Figures 3 and 4 show the frequency dependence of imaginary part of impedance (Z'') at different temperatures for conventional sintered (CS) and microwave sintered (MWS) $Ba(Nd_{0·2}Ti_{0·6}Nb_{0·2})O_3$ ceramics. The value of Z'' decreased with the increase in frequency at lower temperatures in the range 300–698 K (figures not shown in the temperature range, 300–698 K). At lower frequency end,

a slight increase in the Z″ value from 2–4 MÙ for CS sample and 1·5–3·25 MΩ for MWS sample is observed with increase of temperature from 300–673 K. However, as the temperature increased above 673 K (figures 3 and 4), *Z″* value decreased drastically and a broad/diffuse *Z″* peak emerged in frequency for temperatures > 723 K. The broadness/diffuseness of these peaks increases with the increase of temperature. It is also observed that these *Z″* peaks are found to shift towards higher frequency side with the increase of temperature. All the curves merge into single curve for frequencies > 10 kHz in the temperature region, 648–873 K. At higher frequencies, the dispersion due to grain predominates due to the diminishing of the space charge effects, as their relaxation times are very high compared to the grains. The diffuseness of *Z″* peak indicates the distribution of relaxation frequency and the increase in full width at half the *Z″* maximum value with the increase of temperature indicates increase of relaxation frequency distribution. The distribution of relaxation frequency in the present samples may be attributed to cationic disorder due to the random distribution of B-site cations (Nd^{+3}, Ti^{+4}, Nb^{+5}) having different ionic radii and valence states.

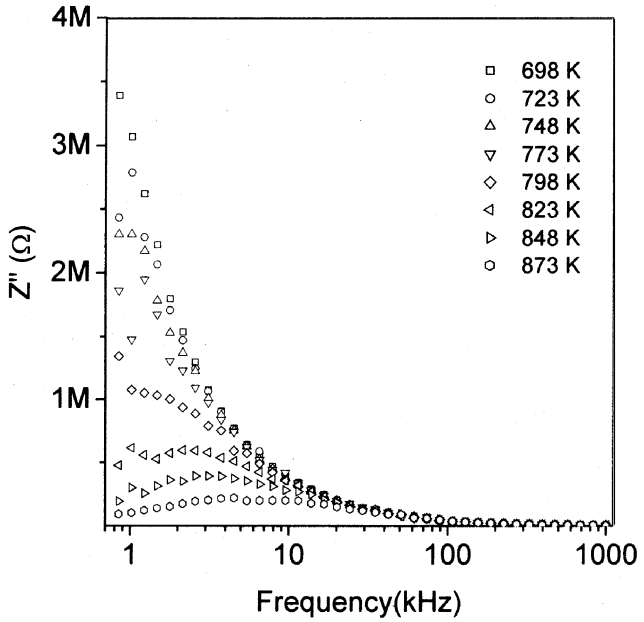

Figure 3. Z″ vs frequency at different temperatures for CS sample.

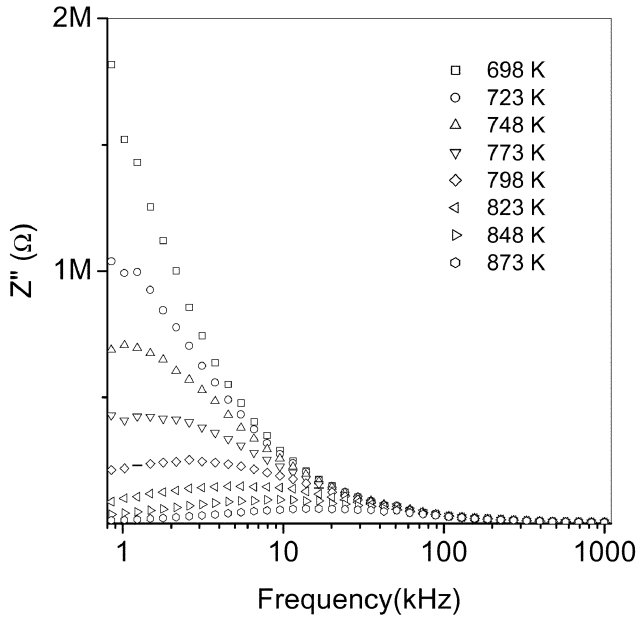

Figure 4. *Z″* vs frequency at different temperatures for MWS sample.

It is also observed from figure 3 for CS sample and figure 4 for MWS sample that in the measured temperature range, *Z″* value for MWS sample (having smaller and uniform grains) is less compared to CS sample (having larger grains). In general, slight amount of oxygen loss occurs in perovskite materials during their sintering at high temperatures and this results in liberation of electrons, which are retained in the crystal structure (Kroger and Vink 1956). Observed impedance/conductivity may be related to the response of these electrons. During cooling of the samples after sintering reoxidation takes place. This oxidation is dependent on the cooling rate. In the case of MWS samples, due to rapid cooling rates less time is available for reoxidation to take place and hence results in more oxygen vacancies/electrons when compared to CS samples where cooling rate is very slow allowing maximum reoxidation to take place. Larger the concentration of oxygen vacancies, due to oxygen loss, larger is the electrons retained in the sample, lower is the impedance, which is in good agreement with our experimental results.

Cole–Cole plots for present sample at different temperatures (in the region 698–873 K) are shown in figures 5 and 6 for CS and MWS samples, respectively. At low temperature range (300–673 K) the plots of *Z″* vs *Z′* linearly line up towards *Z″* axis indicating high resistivity of the samples. With increase of temperature, these graphs curve towards *Z″* axis and for temperatures (≥ 798 K) these curves become almost semicircular type arcs with non-zero high frequency intercept. These high frequency intercepts give the series resistance. The semicircle diameter gives the electrical resistivity of the sample at the specified temperature and the maximum value corresponds to the relaxation frequency, $w = 1/RC$. Initially at low temperatures, when the sample of the resistance is too high, a small portion of the impedance dispersion profile can be detected in the measured frequency range and thus making data analysis impossible. Since, the impedance measurements performed for all the samples below 748 K did not present a complete semicircle, they could not be considered for equivalent circuit modeling in this study.

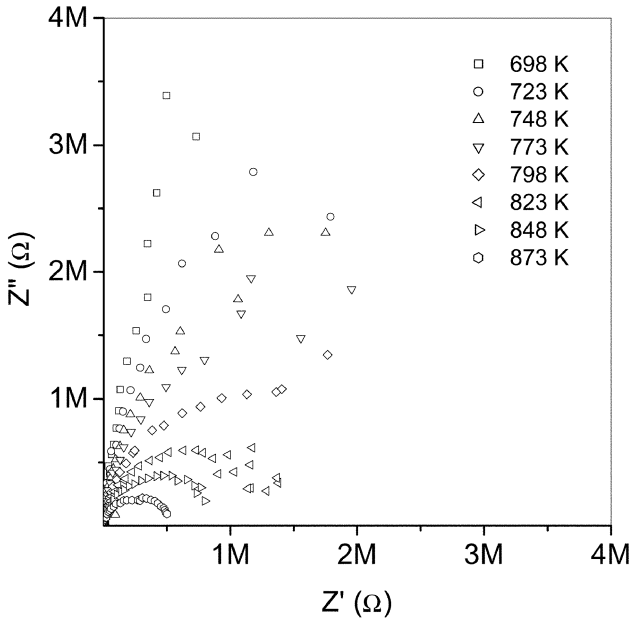

Figure 5. Z^2 vs Z' at different temperatures for CS sample.

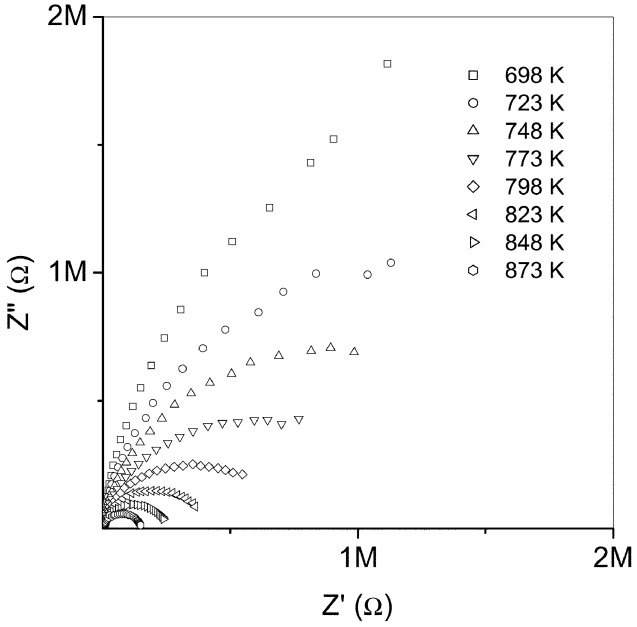

Figure 6. Z'' vs Z' at different temperatures for MWS sample.

The equivalent circuit modeling was done using the equivalent circuit simulation software provided with the AUTOLAB PGSTAT 30 Low Frequency Analyser to separate out grain and grain boundary resistances/capacitances. The equivalent circuit adopted to simulate the experimental data consisted of a simple parallel RC combination in series with resistance, R_s. The fitting is shown in figures 7(a) and (b) along with the experimental data taken at 843 K, for CS and MWS samples, respectively. Single parallel RC combination (R_{bulk}, C_{bulk}) is found to best fit the experimental data for CS sample indicating the contribution from the bulk of the sample and in the measured frequency range, contribution from grain and grain boundaries could not be separated out (figure 7(a)). A series array of two parallel RC combinations [(R_gC_g), ($R_{gb}C_{gb}$)] in series with a resistor (R_s) was found to best fit the experimental data of MWS sample indicating the contribution from grain of the sample and in the low frequency region from the grain boundaries (figure 7(b)). No other relaxation mechanism, such as the electrode effects, is identified in the frequency range studied. Good agreement between the experimental and theoretical curves was observed. The temperature dependence of grain resistance and capacitance of CS sample are illustrated in figure 8(a). Similarly variation of grain and grain boundary resistance and capacitance for MWS sample are illustrated in figures 9(a)–(c). It is observed from figure 8(a) that as the measuring temperature increases, C_{bulk} decreases and also the bulk resistance, R_{bulk}, following a variation of Arrhenius type. The activation energy for bulk conduction in CS sample is of the order of 1·11 eV.

Relaxation frequency for CS sample is calculated from the bulk resistance, R_{bulk} and capacitance, C_{bulk}, using the relation

$$w_{bulk} = 1/R_{bulk}C_{bulk}. \quad (1)$$

The relaxation frequency, w, is known to follow the relation

$$w = w_0 \exp(-E/K_BT), \quad (2)$$

where w_0 is the preexponential relaxation frequency, E the activation energy for relaxation, K_B the Boltzmann constant and T the absolute temperature. The Arrhenius plot of relaxation frequency is shown in figure 8b for CS sample. Activation energy values for bulk relaxation (e_{bulk}), and preterm relaxation frequency (w_{Obulk}) for CS sample are 1·144 eV and $3{\cdot}58 \times 10^{11}$ Hz, respectively.

In the case of MWS sample (figure 9b), the grain capacitance (C_g) decreases with increase of temperature, whereas grain boundary capacitance (C_{gb}) increases with increase of temperature. A slight increase in grain resistance was observed as the temperature increases from 748–798 K (figure 9a), with further increase of temperature from 798 K, grain resistance (R_g) decreases following Arrhenius type, similarly in the measured temperature range, grain boundary resistance (R_{gb}) decreases with increase of temperature following arrhenius type. The activation energy for grain conduction is of the order of 0·94 eV and grain boundary conduction is of the order of 1·31 eV.

Grain and grain boundary relaxation frequencies are calculated from their respective capacitances and resistances, using the relations, $w_g = 1/R_gC_g$ and $w_{gb} = 1/R_{gb}C_{gb}$, respectively. The Arrhenius plot of relaxation frequency is shown in figure 9b for MWS sample. The value of activation energy for relaxation of grain boundary is 1·276 eV and it is found that this value is greater than that for grain relaxation (1·011 eV). Similarly preterm relaxation fre-

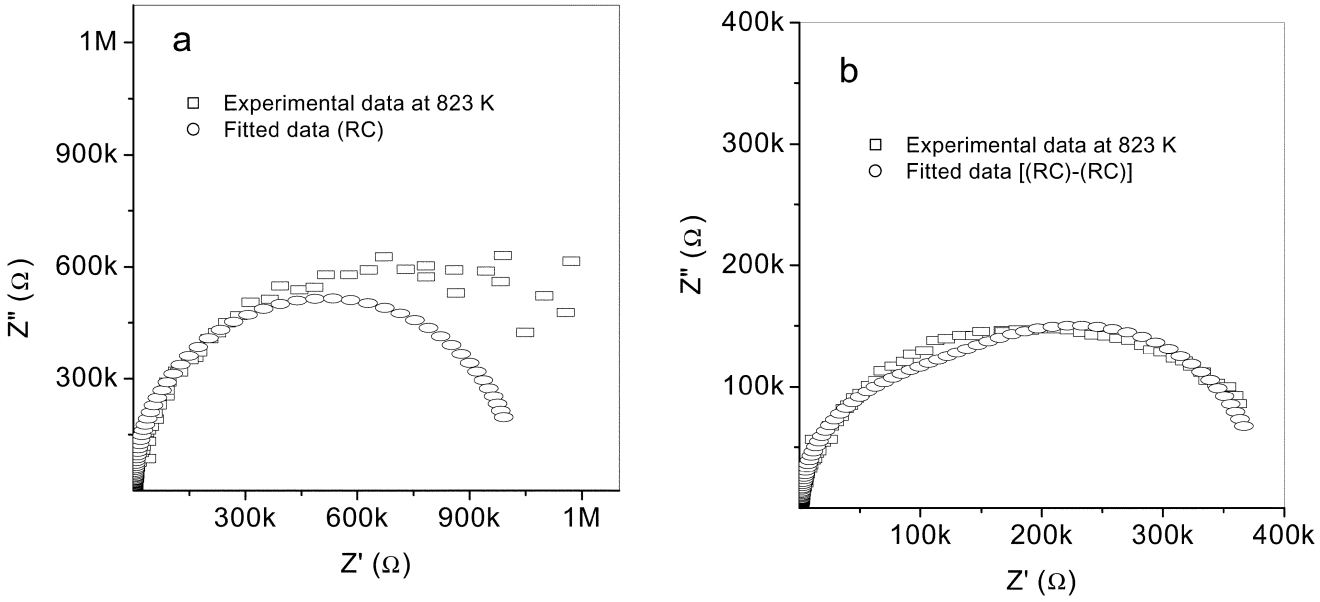

Figure 7. Cole–Cole plots for experimental and fitted curve at 843 K for **a**. CS sample and **b**. MWS sample.

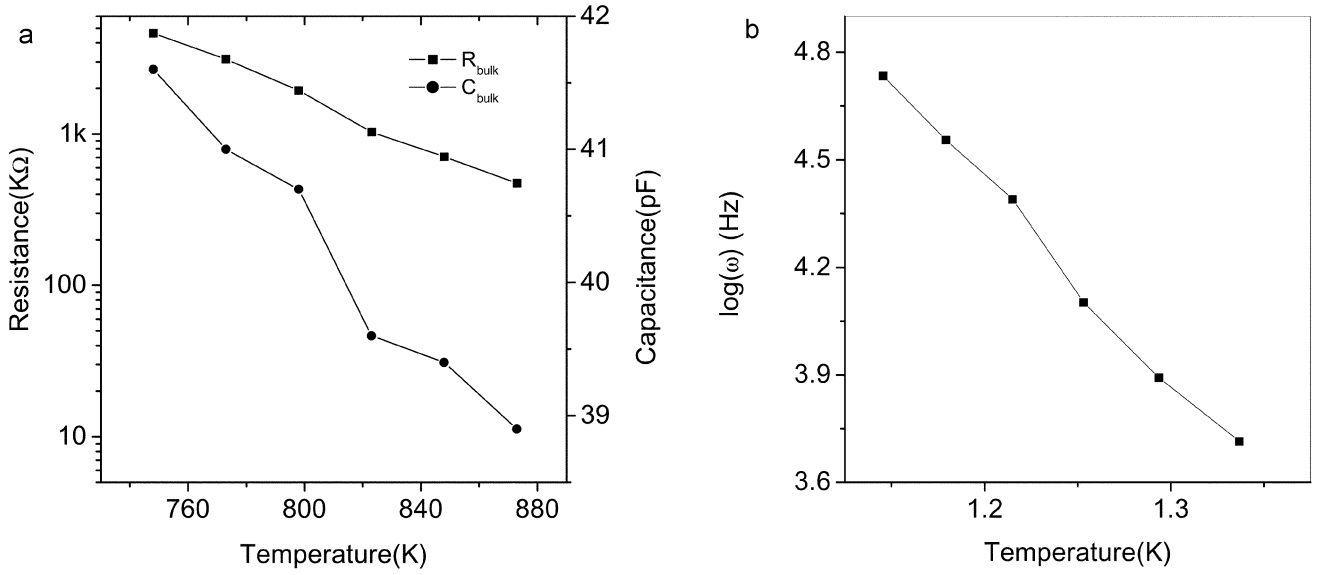

Figure 8. **a**. Grain resistance and capacitance vs temperature and **b**. log(w) vs 1000/T(K) for CS sample.

quency for grain boundary ($1{\cdot}08 \times 10^{12}$ Hz) is one order of magnitude greater than that for grain ($3{\cdot}58 \times 10^{11}$ Hz). It is also observed that the activation energy for grain relaxation is more in MWS compared to CS sample.

The Arrhenius plots for d.c. conductivity are shown in figures 10(a) and (b) for CS and MWS samples, respectively. It is observed that the conductivity increased with increase of temperature and changed by about four to six orders of magnitude in the temperature range investigated. The activation energy values calculated from the slope of Arrhenius plots for conductivity in different temperature regions are presented in table 1. In the case of MWS sample, it is observed that the variation of d.c. conductivity with temperature is not linear and shows a slight change in slope in different temperature regions. This change in slope may be related to the change in conductivity mechanism.

It is reported that titanate based perovskite oxide materials contain Ti^{3+} that are formed because of capture of electron released during the process of formation of oxygen vacancies by Ti^{+4}. The polaronic conduction of 3*d* electrons on Ti^{3+} with low mobility must be predominant at low temperature and these polaronic states are thermally

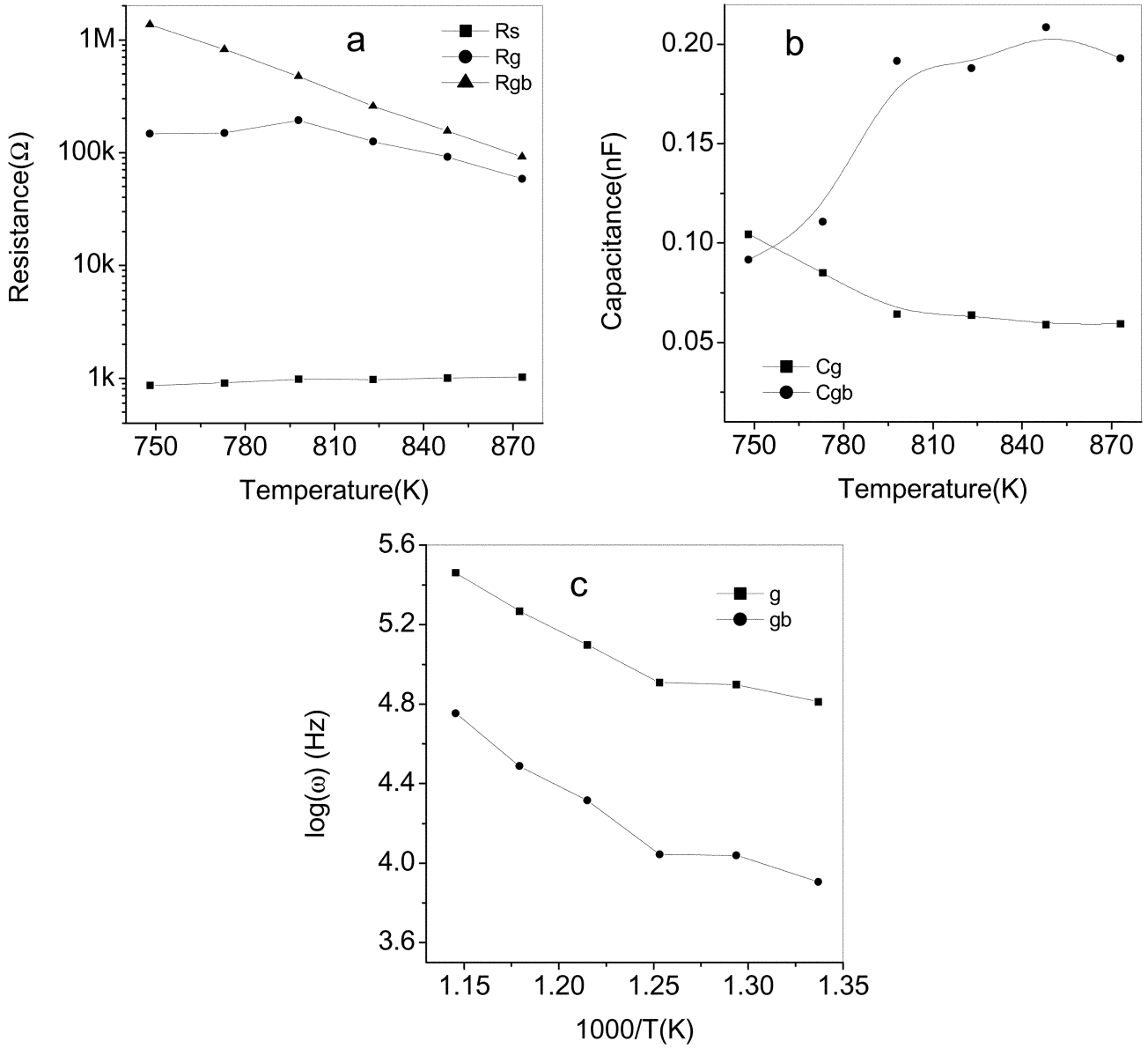

Figure 9. **a**. Series, grain and grain boundary resistance vs temperature, **b**. grain and grain boundary capacitance vs temperature and **c**. log(*w*) vs 1000/*T* for MWS sample.

Table 1. DC and AC conduction activation energies for CS and MWS samples.

	DC conductivity activation energy (eV)			AC conductivity activation energy (eV)					
				11·5 kHz			18·3 kHz		
Sample	Temperature range (K)			Temperature range (K)			Temperature range (K)		
CS	590–770 0·625		770–890 0·955	590–770 0·247		770–890 0·854	590–770 0·117		770–890 0·832
MWS	530–620 0·452	660–750 1·270	775–860 1·658	530–620 0·102	660–750 0·539	775–860 0·844	530–620 0·071	660–750 0·486	775–860 0·739

dissociated and the residual carriers, 3*d* electrons, are strongly scattered by thermal phonons at high temperature, resulting in high electronic conductivity (Iguchia and Mochizuki 2004).

In the present samples, partial replacement of Ti^{+4} ions with Nd^{+3} and Nb^{+5} ions may result in localized oxygen vacancies and titanium vacancies as shown below

$$BaO + TiO_2 \rightarrow Ba + Ti + 3O, \quad (3a)$$

$$6BaO + 3Nd_2O_3 \rightarrow 6BaO + 3Nd_2O_3 \rightarrow$$
$$6Ba + 6Nd_{Ti} + 15O + 3V_O, \quad (3b)$$

$$5BaO + 2Nb_2O_5 \rightarrow 5Ba + 4Nb_{Ti} + 15O + V_{Ti}, \quad (3c)$$

or

$$12BaO + TiO_2 + 3Nd_2O_3 + 2Nb_2O_5 \rightarrow$$
$$12Ba + Ti + 6Nd_{Ti} + 4Nb_{Ti} + 33O + 3V_O + V_{Ti},$$

where V_O is oxygen vacancy having two negative charges, Nd_{Ti} represents the incorporation of Nd at Ti position, Nb_{Ti} represents the incorporation of Nb at Ti position and V_{Ti} is titanium vacancy.

At room temperature and in the low temperature, the d.c. conductivity may be related to the response of the electrons (that are retained during oxygen loss as explained in previous section) and oxygen vacancies to the applied external field. As the temperature is increased thermal fluctuation may dissociate oxygen vacancies into single and double ionized oxygen vacancy with the release of electrons and is given by Kroger–Vink (1956) notation

$$V_O \rightarrow V_O' + e', \quad (4a)$$

$$V_O' \rightarrow V_O'' + e', \quad (4b)$$

where V_O' is single ionized oxygen vacancy having one negative charge and V_O'' is single ionized oxygen vacancy having no net charge on it.

Since Ti can exist in +3 and +4 state, whereas Nb can exist in +4 and +5 states, Ti^{+4} and Nb^{+5} ions may capture the electrons to form Ti^{+3} and Nb^{+3} ions, respectively. The polaronic conduction of 3*d* electrons on Ti^{+3} and 4*d* electrons on Nb^{+3} with low mobility may be predominant at intermediate temperature. These polaronic states may be thermally dissociated and the residual carriers, 3*d* and 4*d* electrons, are strongly scattered by thermal phonons at high temperature, resulting in high electronic conductivity. High electronic conductivity at elevated temperatures may also be attributed to the increase in polaronic conduction. This increase in polaronic conduction may be linked to the formation of more oxygen vacancies due to oxygen loss at very high temperatures. Such type of hopping polaronic conduction has been reported in disordered perovskite, $Sr_{0·97}(Ti_{1-x}Fe_x)O_{3-d}$, by Chen *et al* (1998). Contribution to the polaronic conduction from Nd ion can be ruled out, as it has stable valence state, +3.

Arrhenius a.c. conductivity plots, $\log(s')$ vs $1000/T(K)$, at different frequencies are shown in figures 10(a) and (b) for CS and MWS samples. It is observed from these plots that in low temperature regime, a.c. conductivity increased with increase of frequency indicating dispersion of conductivity with frequency. With increase of temperature dispersion in conductivity narrowed and all the curves for different frequencies appeared to merge into single curve at high temperatures. It has also been observed that the d.c. conductivity of the sample is always lower than the a.c. conductivity and in the low temperature region (400–

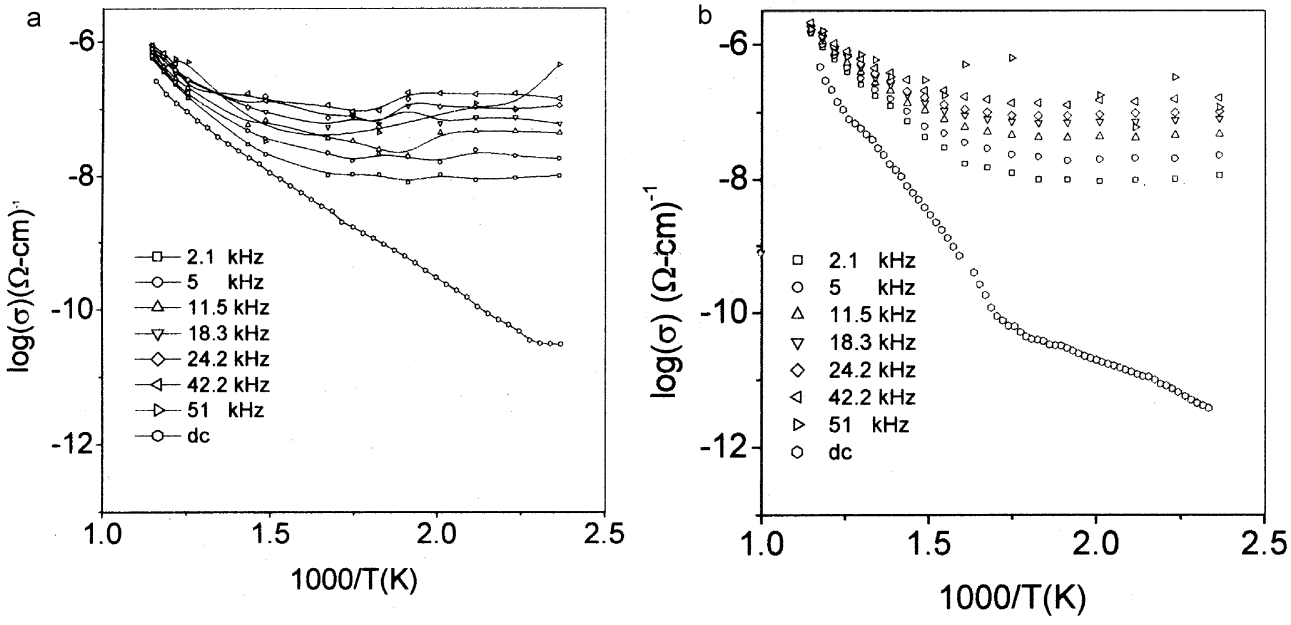

Figure 10. $\log(s'_{a.c.})$ vs $1000/T$ for **a**. CS sample and **b**. MWS sample.

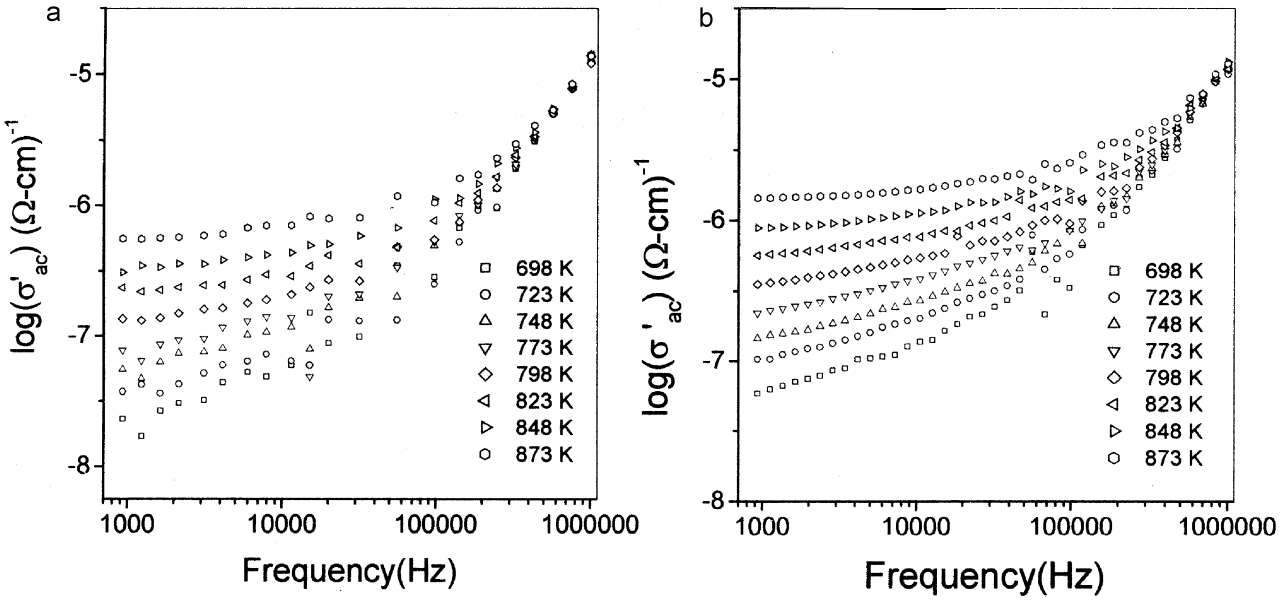

Figure 11. $\log(s'_{a.c.})$ vs frequency for **a**. CS sample and **b**. MWS sample.

600 K), d.c. conductivity is a few orders of magnitude less than the a.c. conductivity and its variation with temperature is also different. This is expected because d.c. conductivity is determined by the most difficult transition in complete percolation paths between the electrodes, while a.c. conductivity is determined by the easiest local movement of the charges. Thus, it is natural to expect that absolute magnitude of these two parameters may not be closely related, and it is evident that their temperature dependence is completely different. The activation energy for a.c. conductivity calculated from the slope of curve of Arrhenius plots at 11·5 and 18·3 kHz in different temperature regions are presented in table 1. The activation energy values are found to increase with the increase in temperature. This may be due to more energy required to overcome the thermal fluctuation by the charge carriers at high temperature region. It is observed that the activation energy values for a.c. conductivity is less than that for d.c. conductivity. It is also observed that a.c. activation energy calculated at high frequency (18·3 kHz) is lower than at low frequency (11·5 kHz) (table 1). This is due to the fact that at low frequencies the overall conductivity is due to the hopping/mobility/transportation of charge carriers over a large distance and at higher frequencies hopping is restricted to only nearest neighbouring defects site, due to smaller response time available to respond to the external field.

The variation of real part of conductivity with frequency is shown in figure 11a for CS sample and in figure 11b for MWS sample. The frequency dependence of a.c. conductivity was characterized using the relation

$$s'(w) = B_1 w^{s_1} + B_2 w^{s_2}, \quad (5)$$

(Funke 1993), where s_1 and s_2 are temperature and frequency dependent parameters and B_1 and B_2 are temperature dependent constants. The parameters, s_1 and s_2, are obtained from the slopes of the plots $\log(s'_{a.c.})$ vs $\log(w)$ in the low and high frequency regions. Thermal variation of parameters s_1, s_2 are shown in figure 12(a, b) for CS and MWS samples. It was found that the value of s_2 is < 2 and the value of s_1 is < 1. It is also observed that the value of s_2 (obtained in the high frequency region) is always more than s_1 (obtained in the low frequency region) in the temperature range investigated. With increase of temperature, the value of s_1, s_2 decreases and the value of s_1 approaches zero at much high temperatures thereby indicating that d.c. conductivity dominates at higher temperatures in the low frequency region.

The frequency response of conductivity is interpreted in terms of the jump relaxation model (Funke 1993; Youssef Ahmed 2002), where the conduction is due to translational hopping for $s_1 < 1$ and localized orientational hopping for $s_2 < 2$. The translational hopping gives the long-range electrical transport (i.e. d.c. conductivity) in the limit of very long times, i.e. as the frequency approaches zero. Since, the values of s_1 and s_2 are within the range specified above over the range of temperature investigated, the conductivity at low frequency may be attributed to the short range translational hopping and the conductivity at higher frequencies may be attributed to the localized orientation hopping or hopping of electron back and forth between two charged defects.

In the present perovskite oxide material the high frequency localized orientation hopping may be attributed to the formation of dipoles, Nb^{+3}–V_O and Ti^{+3}–V'_O. These

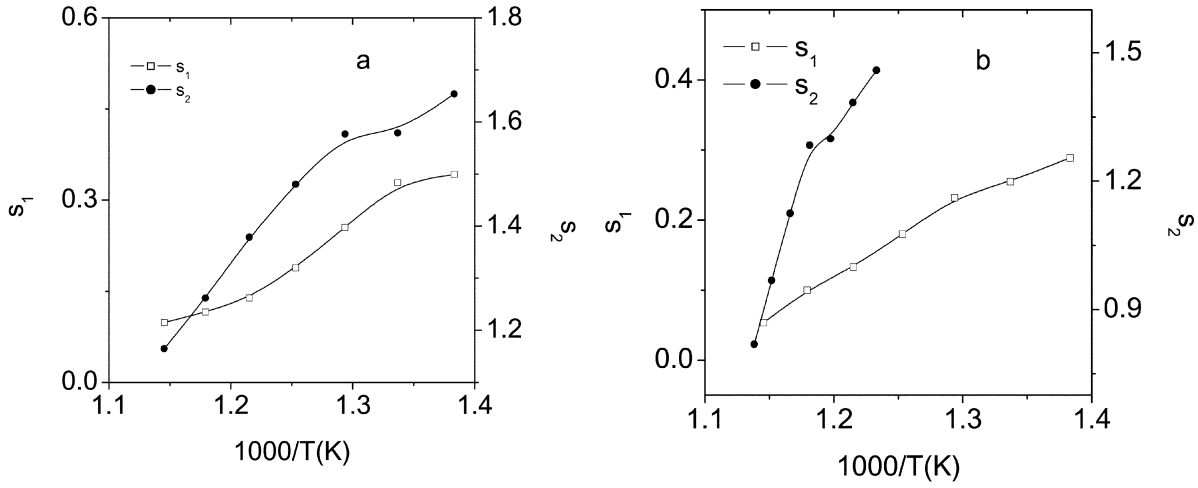

Figure 12. A.C. conductivity parameters (s_1, s_2) vs 1000/T: **a**. CS sample and **b**. MWS sample.

dipoles can change their orientations by electron hopping. The hopping of 4*d* electrons, Nb^{+3}–V_O and Ti^{+3}–V_O', gives rise to localized energy levels in the energy gap of $Ba(Nd_{0·2}Ti_{0·6}Nb_{0·2})O_3$. The charge carriers trapped at these localized sites may form large polarons and conduction occurs as a result of thermally activated large polarons. This is also clear from the temperature dependence of s_1, s_2, which decreases with increasing temperature for hopping mechanism of large polarons (Elliot 1987; Upadhyay 1998).

4. Conclusions

(I) Electrical properties of $Ba(Nd_{0·2}Ti_{0·6}Nb_{0·2})O_3$ prepared through solid state sintering and microwave-sintering route have been studied.
(II) Lower value of Z'' in MWS sample when compared to CS sample was attributed to fast cooling rate in MWS samples. Because of fast cooling rate complete reoxidation do not take place in MWS sample when compared to CS samples and hence electrons that are retained in the crystal structure due to oxygen loss leads to decreased Z'' value in MWS sample.
(III) The frequency dependent imaginary part of impedance indicates distribution of relaxation in the system.
(IV) From equivalent circuit modelling of the impedance data, grain and grain boundary resistance were separated out for microwave-sintered sample.
(V) The Arrhenius plots of d.c. and a.c. conductivity indicate conduction is due to the oxygen vacancies and polarons.
(VI) From a.c. conductivity analysis, the electrical conduction in the low frequency region is attributed to short range translational hopping and at higher frequency region, it is attributed to localized reorientation hopping mechanism.
(VII) The temperature dependence of parameters ($s_1 < 1$, $s_2 < 2$) indicates the hopping is via large polarons.

Acknowledgement

The authors would like to thank DRDO, Delhi, for financial support in carrying out the present research work.

References

Buchanan R C 1988 *Ceramic materials for electronics* (New York and Basel: Marcel Dekker, Inc.)
Chen Ang, Jurado J R, Yu Zhi, Colomer M T, Frade J R and Baptista J L 1998 *Phys. Rev.* **B57** 11858
Chen Ang, Yu Zhi and Jing Zhi 2000 *Phys. Rev.* **B61** 957
Elliot S R 1987 *Adv. Phys.* **36** 135
Funke K 1993 *Prog. Solid State Chem.* **22** 111
Iguchia E and Mochizuki S 2004 *J. Appl. Phys.* **96** 3889
Kroger F A and Vink H J 1956 *J. Solid State Phys.* **3** 307
Mahboob Syed, Dutta A B, Swaminathan G, Prasad G and Kumar G S 2005 *Ferroelectrics* **326** 79
Park Seung Eek, Wada Satoshi, Cross L E and Shrout Thomas R 1999 *J. Appl. Phys.* **86** 2746
Senda Said and Mercurio Jean-Pierre 2001 *J. Eur. Ceram. Soc.* **21** 1333
Seok Hyun and Kim Hwan 1999 *Jpn J. Appl. Phys.* **38** 4824
Sheets Sossits A, Soukhojak Andrey N, Ohashi Naoki and Chiang Yet-Ming 2001 *J. Appl. Phys.* **90** 5287
Sinclair D C and West A R 1989a *J. Appl. Phys.* **66** 3850
Sinclair D C and West A R 1989b *Phys. Rev.* **B39** 13486
Suchanicz J, Gavshin M G and Kudzin A Yu 2001 *J. Mater. Sci.* **36** 1981
Upadhyay Shail, Sahu Ashok Kumar, Devendra Kumar and Om Parkash 1998 *J. Appl. Phys.* **84** 828
Wang Xiaoxing, Helen Lai-Wa Chan and Chung Loong Choy 2003 *Solid State Commun.* **125** 395
Youssef Ahmed A A 2002 *Z. Naturforsch.* **A57** 263
Yu Zhi, Guo Ruyan and Bhalla A S 2000 *J. Appl. Phys.* **77** 1535